UNIVERSIDAD
NACIONAL
DE COLOMBIA

Fault diagnosis mechanism of gears and bearings for coal mining equipment in a complex geological environment

Shuilin Wang[1,2*], Songyong Liu[1], Fanping Meng[3]
[1]School of Mechatronic Engineering, China University of Mining and Technology, Xuzhou, 221116, China
[2]Xuhai College, China University of Mining and Technology, Xuzhou, 221008, China
[3]Yongcheng Coal & Electricity Holding Group Co. LTD, Shangqiu, 476600, China
*Corresponding author: wslxhxy2008@163.com

ABSTRACT

The traditional research method of fault diagnosis mechanism has poor stability, which leads to the difference of fault diagnosis and location results. Therefore, under the complex geological environment, a new research method of fault diagnosis mechanism of gear and bearing for coal mining equipment is proposed. This method calculates gears and bearings' yield strength by analyzing coal mining equipment's bearing capacity elasticity. According to the fitting degree, the equipment sample's projection space is confirmed, the fault features of gear and bearing are extracted by segmentation algorithm, the optimal fitness is set by positioning algorithm, the location of fault center is obtained, and the fault mechanism diagnosis is studied. Experimental results show that compared with the traditional method, the proposed method is more stable, and the difference in fault diagnosis results is minimal. It can be seen that this method is more suitable for fault diagnosis of coal mining equipment.

Diagnóstico de fallas de engranajes y cojinetes para equipos de minería de carbón en entornos geológicos complejos

RESUMEN

El método de investigación tradicional del mecanismo de diagnóstico de fallas tiene poca estabilidad, y puede conllevar a diferencias entre el diagnóstico de fallas y los resultados de ubicación. Por lo tanto, en un entorno geológico complejo se propone un nuevo método de investigación del mecanismo de diagnóstico de fallas de engranajes y cojinetes para equipos de minería de carbón. Este método calcula el límite elástico de engranajes y cojinetes al analizar la elasticidad de la capacidad de carga de los equipos de minería del carbón. De acuerdo con el grado de ajuste, se confirma el espacio de proyección de la muestra del equipo, las características de falla del engranaje y el cojinete se extraen mediante un algoritmo de segmentación, la aptitud óptima se establece mediante el algoritmo de posicionamiento, se obtiene la ubicación del centro de falla y se estudia el mecanismo de diagnóstico de falla. Los resultados experimentales muestran que, en comparación con el método tradicional, el método propuesto es más estable y la diferencia entre los resultados del diagnóstico de fallas es muy pequeña. Se puede ver que este método es más adecuado para el diagnóstico de fallas de equipos de minería de carbón.
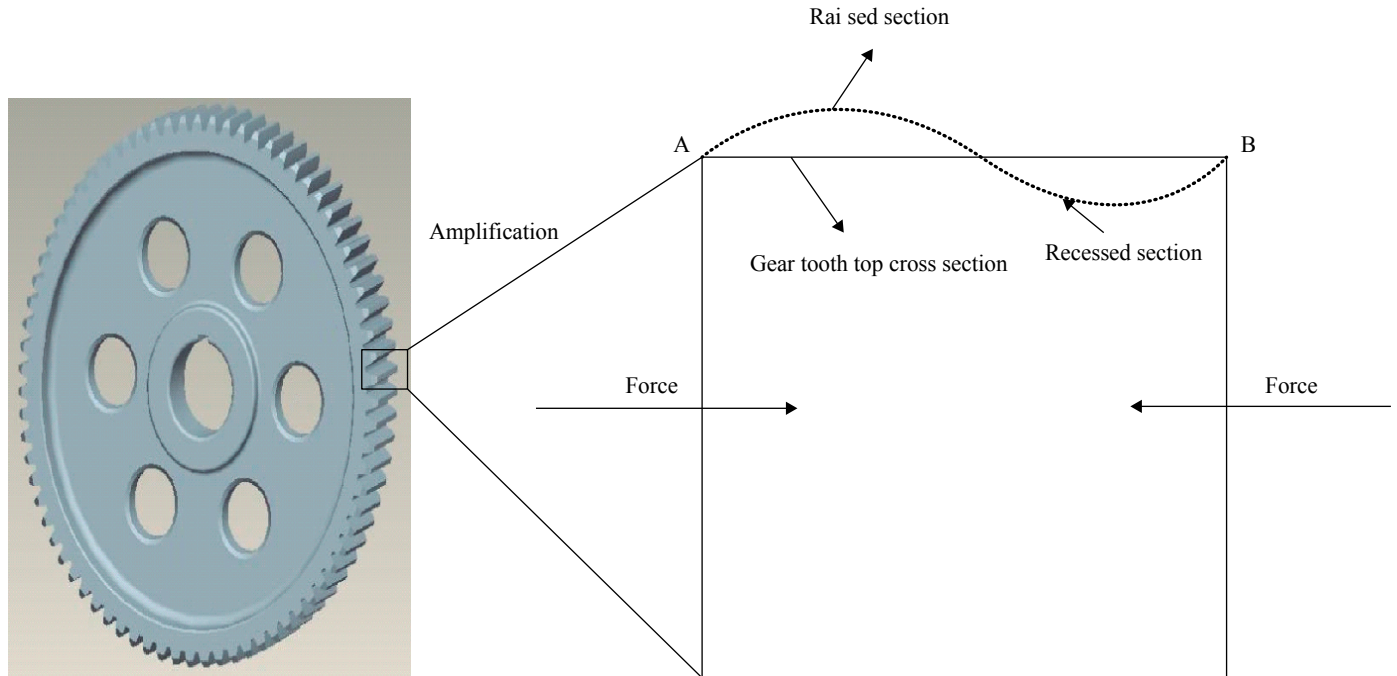
Figure 1. Schematic diagram of the elastic load capacity of the gear

Introduction

With the rapid progress of science and technology and the continuous improvement of modernization, coal mining equipment is increasingly developing towards the direction of large-scale, integrated, high-speed, precise and intelligent. With the development trend of mechanical equipment, it is the complexity of equipment. The relationship between different equipment and different parts of the same equipment is more complex, forming a unified whole. When any one of the components fails, not only the operation of the equipment itself, but also the operation of other equipment associated with the equipment will be affected, which will cause a series of chain reactions, resulting in the interruption of the operation of the whole equipment, affecting normal production and product quality. On the other hand, affected by the geological conditions and hydrological environment of coal mining, under the complex natural environment, the mining difficulty of coal mining equipment is greatly increased. Excessive operation makes the gears and bearings in the equipment prone to failure. Therefore, through real-time monitoring of the working conditions of gears and bearings, the traditional research methods, obtain the operation parameters of parts, and statistics the fault location through the difference method, to find the nodes prone to failure and the time of failure. It is found that the signal of the fault location is unstable due to the poor ability to analyze the fault characteristics, which makes the accuracy of the fault mechanism decline. Therefore, a new fault diagnosis mechanism research method is proposed. According to the relationship between gears and bearings, the method resets more stable fault feature extraction and location according to the acquisition method of cyclostationary signal and projection decomposition operation method to ensure the reliability of fault diagnosis mechanism (Morris et al., 2018). This method not only solves the existing problems of the traditional methods, but also provides scientific and technical solutions for the fault diagnosis mechanism research of gears and bearings in other fields, and provides reasonable research methods for the development of national equipment and technological innovation.

Research method of fault diagnosis mechanism of gears and bearings for coal mining equipment in complex geological environment

Calculation of yield strength of gears and bearings in complex geological environment

On the basis of defining the basic parameters of a complex geological environment, the yield strength of gears and bearings is calculated. As all gears and bearings will not be perfect, under the influence of a complex mining geological environment, the top of gears may buckle within a reasonable range due to the influence of bearing force during operation (Balestro et al., 2018). Therefore, to determine the directional elasticity of the stability of gears and bearings, the method of angular displacement can be used for directional analysis. Under the complicated geological conditions, the equation of angular displacement of gears after bearing the axial force is as follows:

$$\begin{cases} \beta_A = f\left[a\mu_A + b\mu_B - \dfrac{\lambda(a+b)}{d}\right] \\ \beta_B = f\left[b\mu_B + a\mu_A - \dfrac{\lambda(a+b)}{d}\right] \end{cases} \quad (1)$$

In the formula, f represents the linear stiffness of the bearing, $f = EI/d$, d represents the size of the gear, A and B represent the left and right ends of the gear respectively, β_A and β_B represent the angular displacement of the two ends of the gear, μ_A and μ_B represent the deformation angle of the two ends of the gear respectively, λ represents the lateral displacement value of the bearing, a and b represent the stability function and the bending stiffness coefficient. Figure 1 is a schematic diagram of the gear tooth deformation curve under the axial force.

In the figure above, it is the displacement of a single gear tooth after deformation, and the critical load can be calculated only according to the

balance equation. However, the fault situation shown in the figure is relatively simple. Under the condition of bearing and gear tooth deformation, the tooth slot will also be deformed. Therefore, the shear balance equation should be established to solve the elastic buckling load. Figure 3 is the structural diagram of the gear after the deformation of the teeth and grooves. Assuming that there is vertical load on the axis at the upper and lower ends of the structure, it is represented by p_1 and p_2 (Wang et al., 2018).
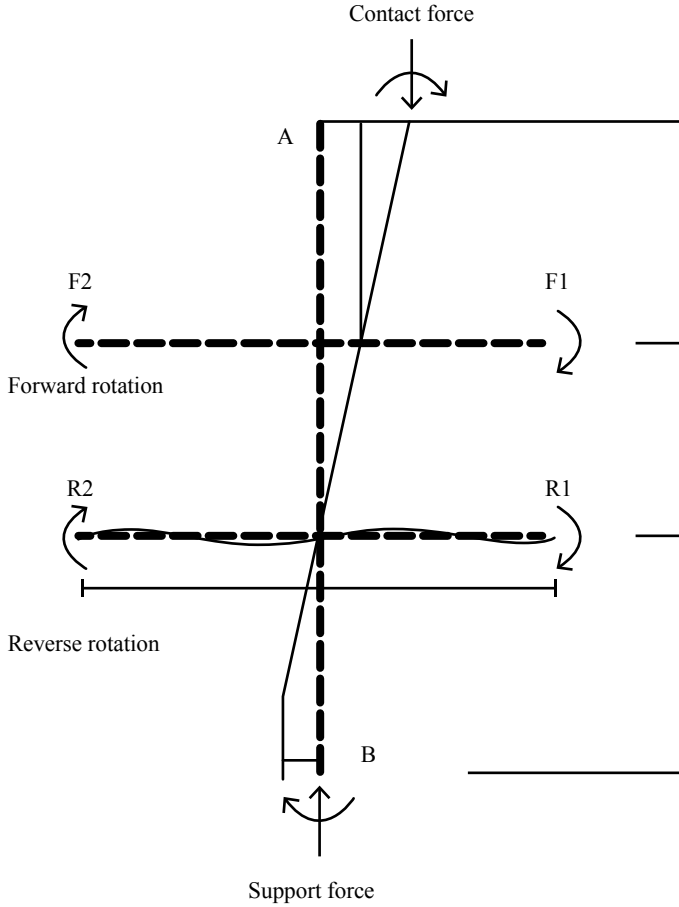

Figure 2. Schematic diagram of the load structure of the gear under the load

According to the above figure, in order to facilitate the analysis of the load elasticity of the gear, it is assumed that the A and B ends of gear M_i buckle at the same time with the other gear M_j in contact with each other, and that AA' and BB' are the contact ends. At this time, the end angles of the cross section in the same layer of gear are the same size and opposite direction, that is, $\alpha_A = -\alpha_{A'}$, $\alpha_B = -\alpha_{B'}$. It is known that the k value between the gears is the same, and the bending stiffness coefficients are both a and b. By default, the gear in the same layer buckle at the same time when losing stability. Then, according to Formula 1 and the balance condition $p_1 = -\lambda p_2$, the elastic value of the bearing capacity of the gear slot under the tooth deformation is calculated by using the angle displacement method.

$$\begin{cases} F_{AA'} = \dfrac{EI_{M_i}}{k_1}\left[a\beta_A + b\beta_B - (a+b)\lambda\eta\right] \\ F_{BB'} = \dfrac{EI_{M_j}}{k_2}\left[a\beta_B + b\beta_A - (a+b)\lambda\eta\right] \end{cases} \tag{2}$$

In the above formula, k_1 represents the elastic value of bearing capacity of contact point AA', k_2 represents the elastic value of bearing capacity of contact point BB', EI_{M_i} represents the transfer force of target gear M_i,

EI_{M_j} represents the bearing force of gear M_j adjacent to M_i, η represents the force balance coefficient, and λ represents the force control coefficient. It is known that the sum of equilibrium conditions of node A and node B is 0, and there is $F_{AA'} = -F_{BB'} + \Delta F$, that is, $F_{AA'} + (-F_{BB'}) + \Delta F = 0$, where ΔF is the force of other values. According to the equilibrium condition, let $K = (k_1 + k_2)^2$, thus, the instability condition of gear under high strength operation is as follows:

$$sK\left(\frac{|F_{AA'}| + |F_{BB'}|}{2}\right) - (mh)^2 = 0 \tag{3}$$

In the formula, s represents the linear stiffness of the gear under the action of external force, m represents a non-zero natural number, and h represents the constraint condition. The trigonometric function is substituted to the above formula, and $\varphi = \sqrt{\dfrac{f}{EI}}\,/\,mh$ is made to obtain the buckling equation of gear teeth and bearings:

$$sK\left(\frac{|F_{AA'}| + |F_{BB'}|}{2} - \varphi^2\right)\tan\varphi + \frac{\varphi}{K} = 0 \tag{4}$$

Where φ is the buckling evaluation parameter. The above equation is the elastic analysis equation of bearing capacity of gear and bearing. It should be noted that the bearing will also be affected by the horizontal load force, so under the condition of meeting the above formula, the elastic calculation expression of gear shear balance is:

$$K' = \frac{EI}{d} \times \frac{(a+b)(a-b+ab)}{b+c} \tag{5}$$

In the formula, c represents the constant of change under the influence of bending stiffness coefficient a and b, and EI force modulus. When K' is greater than the specified elastic value, it means that the gear is distorted under the influence of load. Under the influence of Formula 5, the plastic value of the bearing capacity of the false gear is set as f, and when the value of f exceeds the maximum limit of the gear, the yield strength of the gear is calculated. According to the yield strength value, the critical value of functional failure of gear bearing capacity is confirmed. The basic material composition of the gear is known, and the amplification coefficient of the compressive strength of the material is calculated. The formula is:

$$CDIF = \frac{P_1}{P_2} = \left[\frac{e_1}{e_2}\right]^{\vartheta} \tag{6}$$

In the formula, e_1 represents the strain rate and $e_1 \geq 30s^{-1}$, e_2 also represents the strain rate and $e_2 = 30 \times 10^{-6}s^{-1}$; P_1 represents the dynamic compressive strength of the material under e_1, P_2 represents the static compressive strength of the material under e_2; $\vartheta = \left(\dfrac{3P_3 + u}{4}\right)^{-1}$ represents the force angle under impact, wherein P_3 represents the compressive strength under the total volume of the material (Jeong et al., 2018). The increase coefficient of tensile strength is:

$$TDIF = \frac{Q_1}{Q_2} = \left[\frac{\tau_1}{\tau_2}\right]^{\sigma} \tag{7}$$

In the formula, τ_1 represents the strain rate under the influence of the force, $\tau_1 \leq 1s^{-1}$, τ_2 represents the strain rate under the influence of the force, and $\tau_2 = 10^{-6}s^{-1}$; Q_1 represents the dynamic tensile strength of the material composed of gears under τ_1, Q_2 represents the static tensile strength of the material under τ_2; $\sigma = 10^{-6n-2}$ represents the force angle, where

$n = \left(\dfrac{1+8Q_3 1}{Q_0} \right)^{-1}$, Q_3 represents the standard static tensile strength that the material can bear, Q_0 Represents the static tensile strength of a variable material. By combining the Formulas 6 and 7, the yield strength calculation formula is obtained

$$z = \left[1 + \tau f \left(\frac{\omega}{m} \right)^{\frac{1}{j}} \right] \left(z_0 + \alpha E_j \omega^{eff} \right) \tag{8}$$

In the formula, z_0 represents the initial yield stress, τ represents the strain rate, ω^{eff} represents the equivalent plastic strain, E_j represents the plastic hardening modulus, α represents the hardening parameter, when $\alpha = 0$ represents the follow-up strengthening, m and j represent the constants respectively. When $z < 0.7$, it means that the frame gear can bear the current working strength, the gear is in good condition, and the bearing capacity function has not been lost; when $0.7 \leq z \leq 0.8$, it means that the gear can bear the current working strength, but affected by the geological conditions, at this time, the gear has the situation of tooth section depression or external convex, and part of the bearing capacity function; when e > 0.8, it means that the gear is seriously deformed or the gear teeth are directly broken, unable to withstand the current operation, and the bearing capacity function of the gear is completely lost (Walker et al., 2018).

Extraction of gear and bearing fault features

The real-time running state of the bearing is obtained by using the monitoring system. It is known that the monitoring data will be distorted due to salt and pepper noise, Gaussian noise and reflected half point noise in the process of recording and transmission. Therefore, the bearing monitoring data is estimated by using the geometric shape analysis method and digital analysis method of mathematical concept. Through the analysis of the relationship between the elements, the bearing monitoring data is estimated, and the linear least square method is used to measure the impact of noise on the data, that is, according to the calculated minimum average variance, the monitoring background that can be fitted is determined. Therefore, the calculation formula of the fitting degree is:

$$f(x) = k_1 x + k_2 x + k_3 x + k_4 x \tag{9}$$

In the formula, k_1, k_2, k_3 and k_4 are respectively represented as the influence of background information on noise in each direction, and x is the mutation value of noise (Spartalis et al., 2018). The average variance is calculated according to the Formula 9:

$$S^2 = z \sum_{i=1}^{n} \left[X_i - k_i(x) \right]^2 \tag{10}$$

In the formula, X_i represents the gray value of the i-th column of the monitored data. At this time, the calculation result is the noise factor of background information in four positive directions. Due to the inaccurate fault location and calculation deviation, the information interference in other directions is corrected by information extraction, and the median filter is weighted and added. At this time, the corrected background noise estimate is:

$$V = u_1 \gamma^2 + u_2 w \tag{11}$$

In the formula, according to the γ^2 value obtained by the above fitting, w represents the median filter, u_1 and u_2 represent the weighting coefficient, and $u_1 + u_2 = 1$, so as to obtain a more accurate noise background. According to this value, the interference noise is proposed, and the complete bearing monitoring data is obtained. In order to detect the defects of the pre-processing monitoring data, it is necessary to determine the fault area and segment it. According to the monitoring data, ROI is the region of interest. The bearing in this region is judged and segmented according to the result. According to the imaging principle, known bearings can be divided into three areas: the upper background area, the middle imaging area and the lower turntable area (Ganson, 2018). According to the principle of uniform direction and gray projection algorithm, the distribution rule of bearing projection is analyzed to determine the scope of fault analysis. According to the above calculation results, the gray projection on the calculation axis is:

$$g(y) = \frac{1}{V} \cdot \sum_{i=1}^{V} h(x, y) \tag{12}$$

In the formula, V is the background value calculated by Formula 11, $h(x, y)$ is the projection normal distribution function. According to the calculation results, the curve characteristics are analyzed, to determine the bearing monitoring data on the y-axis of the imaging boundary. Figure 3 is the sample space schematic diagram of the projection curve.
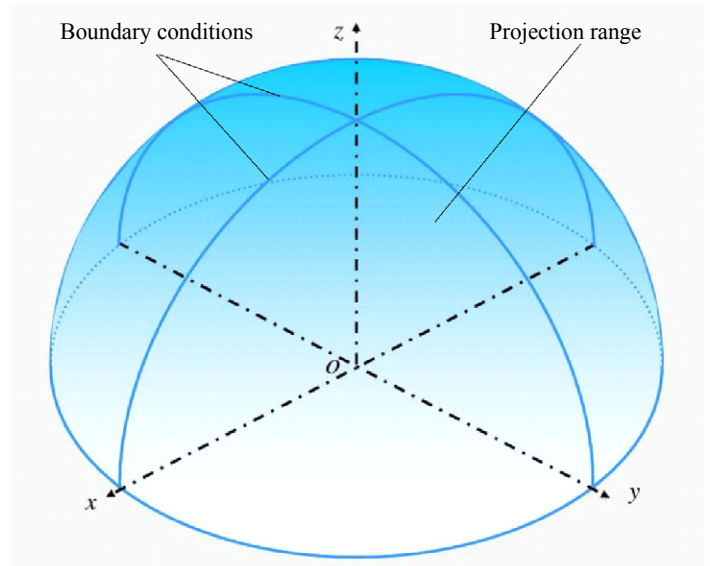

Figure 3. Sample curve projection space

The two curves in the image are the constraint conditions for generating projection curves for non damaged samples, scraped samples, bumped samples and over sharpened samples. It is known that no matter what type and specification of the bearing for coal mining equipment, its projection shape is similar, the upper background area has no detection objects, and there is no effective monitoring data; the bottom area has a certain degree of fluctuation because of the problem of reflection; the middle position is the main data monitoring area of the bearing, because the bearing itself is smooth, there will be reflection phenomenon, thus, the curve of this projection will fluctuate violently. According to the above analysis results, the region ROI calculation algorithm is set up: the gray projection curve is filtered by means of mean value, and the curve is derived by smooth value, so that it passes through the zero point, and then the maximum value point and secondary value point of the curve are found out from the zero point, the abscissa is set as x_1 and x_2, and $(0, c_1)$ and $(0, c_2)$ are taken as control points to establish a rectangular region, which is ROI (Liu & Zhu, 2018).

Because the image boundary of the bearing in the ROI area at this time is relatively fuzzy, which will affect the classification of defect categories, the wave value transformation segmentation algorithm is adopted to accurately segment the image area of the bearing, as shown in Figure 4.
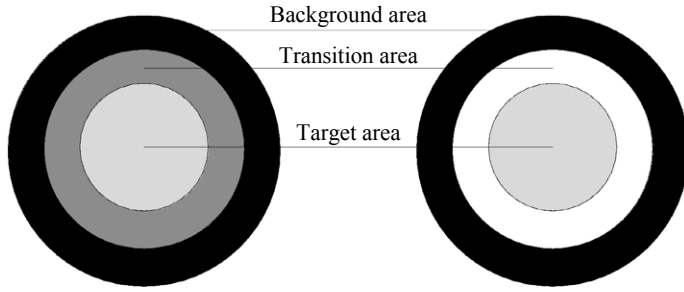
Figure 4. Schematic diagram of the segmentation process

It can be seen from the figure that there may be errors in the boundary of the segmented region. One is to divide the background into the target region, and the other is to divide the target pixels into the background region. In order to avoid such a situation, morphological processing is carried out. Morphological treatment is to expand and corrode. Expansion is to merge all the contact points of the object's contact background into the object, so that the boundary expands outwards, while corrosion is to eliminate the fictitious contact points, so that the boundary contracts inwards. The calculation process is as follows:

$$\begin{cases} U_2 - U_1 = S_1 \\ W_1 - W_2 = S_2 \\ U_1 - W_1 = S_3 \end{cases} \tag{13}$$

In the formula, U_1 and U_2 represent the area obtained by two expansions, W_1 and W_2 represent the area obtained by two corrosions, S_1 represents the part around the boundary that does not belong to the target range, S_2 represents the area around the boundary that belongs to the target range, S_3 represents the area that cannot be determined, so the area is divided into bundles. On the basis of region segmentation, the feature statistics and extraction of these data are carried out, and the rule subsets are established according to these features, so as to reduce the deposition data and improve the accuracy of fault diagnosis. The shape feature of gears and bearings in coal mining equipment is one of the important features of fault identification, so the common fault shape feature shown in Table 1 below is listed (Ali et al., 2018).

Table 1. Basic shape characteristics when gears and bearings fail

Serial number	Characteristic shape	Feature description
1	Area	Amount of data in the split area
2	Perimeter	Amount of data in adjacent divided regions
3	Diameter	The horizontal distance between the two furthest data points on the boundary
4	Center of gravity	Horizontal center of gravity, vertical center of gravity
5	Aspect ratio	Aspect ratio
6	Number of cracks	Easy to describe and quickly calculated values in the segmented area
7	Thin length	Ratio of perimeter to area, ratio of diameter to area
8	Compactness	Data to measure the complexity of the boundary
9	Similarity	Ratio of vectors
10	Symmetry	Symmetric distance after region rotation

According to the data in Table 1, the bearing deformation features are extracted. It is known that the color distribution of bearings and gears is divergent under the condition of light source, light and object reflection in machine vision. Assuming that the hue is M, the saturation is D, and the brightness is R, the color distribution is calculated:

$$\propto = \left(E + \frac{m}{M} \right) + \sum_{i=1}^{n} \sqrt{\left(\frac{D_{\max} - D_{\min}}{D_{\max} + D_{\min}} \right)} + \ln\left(1 - \frac{|R - 0.5|}{0.5} \right) \tag{14}$$

In the formula, E represents the parameters of the segmented area, and m represents the hue resolution. Through the color resolution model, the color features of gear and bearing images are obtained, and then the texture features are counted. Because the change of texture image has certain regularity, which is embodied in the attributes of density, thickness, uniformity, regularity, linearity, frequency, etc., according to these attributes, the image area is set as $W(x,y)$, the size is $i \times j$, and the calculation formula is as follows:

$$\begin{cases} i = \sum_{i=1}^{n} x_i f\left(x_i \right) \\ j = \sum_{i=1}^{n} [x_i - i] f\left(x_i \right) \end{cases} \tag{15}$$

In the formula, x_i represents the gray level series, $f\left(x_i \right)$ represents the probability function of gray level series, which is the statistical result of texture features. In the process of feature extraction, it is necessary to make the selected features meet the separability constraints, which is to be representative, so that they can not only reflect the characteristics of all aspects, but also reflect the personality of the object; secondly, the graphic features should have very strong anti-interference, so as to ensure that the influence of different lighting, light source, shape and other factors is small and stable, the feature values of image content in the segmentation region are similar, and the selected features are independent of each other. In this paper, the scale feature extraction method is used to extract data based on the statistical results of features. The image is transformed to another space by function or matrix. The transformation methods include frequency domain transformation and geometric projection transformation. The data with different functional features in feature grouping are extracted and a new feature set is established. According to this feature, the calculation results are as follows:

$$\varepsilon = \sqrt{\mu \zeta_n \cdot \left(\kappa^2 \cdot i + \kappa^2 j \right)} \tag{16}$$

In the formula, ζ_n represents n shape values, κ, i and j are the result statistics values of formula (2-7), so as to realize the extraction of gear and bearing fault feature data in coal mining equipment in a complex geological environment (Sayers et al., 2019).

Fault location parameters setting of the location algorithm

On the basis of defining the fault characteristics of gears and bearings, the fault location algorithm is developed according to the basic operation mode of coal mining equipment. Generally speaking, the first step is to determine the fault range of gears and bearings. Using CS technology to set up a search program, the target range of fault location is defined. The step factor is calculated, which is the key parameter to control the breadth of the search area. When the step factor is too large, the search program is controlled to start a full regional search; when the step factor is too small, the parameter can control the search program to start a local search in a local area. In order to control the search balance of the search program in the whole region and the local region, a balance adaptive adjustment parameter is added to make the search program distributed and synchronous search. The calculation formula of the step factor is:

$$r_s = r_{max} - \frac{k(r_{max} - r_{min})}{\tau n} \times \frac{f_1 - f_2}{f_1} \tag{17}$$

In the formula, r_s represents the search step of the s-th time, where s represents the current number of times; k represents the control parameter; r_{max} represents the maximum upper limit of step factor; r_{min} represents the minimum lower limit of step factor; τ represents the adjustment parameter introduced; n represents the maximum number of iterations; f_1 represents the optimal function under the initial fitness; f_2 represents the optimal function suitable for this iteration. At the same time, under the search control of this parameter, the discovery probability of the approximate location of the equipment fault is calculated. In CS technology, the discovery probability is generally between 0.2-0.3, and the probability under this parameter is set to p. When the probability is always in a large value, the convergence speed of the fault search can be accelerated; when the value of the discovery probability p is small, the convergence rate is reduced. Therefore, the optimal fitness is set by the ratio of the optimal fitness and the previous generation solution.

$$f = \begin{cases} 1 & f_i > f_{ri} \\ 0 & f_i \le f_{ri} \end{cases} \tag{18}$$

In the above formula: f_i represents the optimal fitness of the previous generation; f_{ri} represents the fitness of the i-th solution under the action of r_s. According to the above calculation formula, the detection probability calculation results obtained by adjusting the adaptability of the detection probability are as follows:

$$\begin{cases} p' = \sum_{i=1}^{N} d_i / f \\ p = p_{min} + (p_{max} - p_{min}) \cdot p' \end{cases} \tag{19}$$

In the formula, p' represents the high-quality probability of the solution after iteration; d_i represents the optimal fitness for the i-th solution; N represents the total number of solutions; p_{min} and p_{max} represent the upper and lower limits of the discovery probability respectively. Combining the above two sets of formulas, the search parameters are obtained, and the capture function is set by the parameters to extract the fault nodes of gears and bearings within the range of the target. According to the carrier frequency of the data, the capture function can get the code phase of the defect data and realize the acquisition of data nodes in any area. The capture times of the capture function are calculated as follows:

$$n = j_1 \times \left(2 \times \frac{d}{j_0} + b \right) \tag{20}$$

In the formula, n represents the number of acquisition times, j_i represents the number of times of code phase, j_0 represents the total step of wave frequency, d represents the step of wave frequency of defect data, and b represents a fixed constant, usually 1. The capture function is set according to the capture times, and the capture parameter $f(x)$ is introduced, as follows:

$$\begin{aligned} DFT &= \int_0^t [f(x)] q^{-a2\pi st} dx \\ &= W_n(s) \int_0^t [g_f(t)] q^{a2\pi st} dx \\ &= W_n(s) W_f^*(s) \end{aligned} \tag{21}$$

In the above calculation expressions, DFT represents the Fourier calculation result of the acquisition function under the condition of discrete transformation; q represents the degree of acquisition; x represents the independent variable of the acquisition function; q represents the exponential function; a represents the frequency of acquisition; s represents the conjugate value; t represents the target range space; $g_f(t)$ represents the real-time fault signal; $W_n(s)$ represents the fixed value of the acquisition strength of the fault signal under n times of acquisition; $W_f^*(s)$ indicates the actual acquisition strength of fault data when the acquisition strength is f, * indicates the transformation flag. In the obtained defect nodes, two adjacent defect nodes are randomly selected as samples, to calculate the defect center point by distance scaling method, and the fault sample curve is selected, as shown in Figure 5 (Heffner et al., 2018).
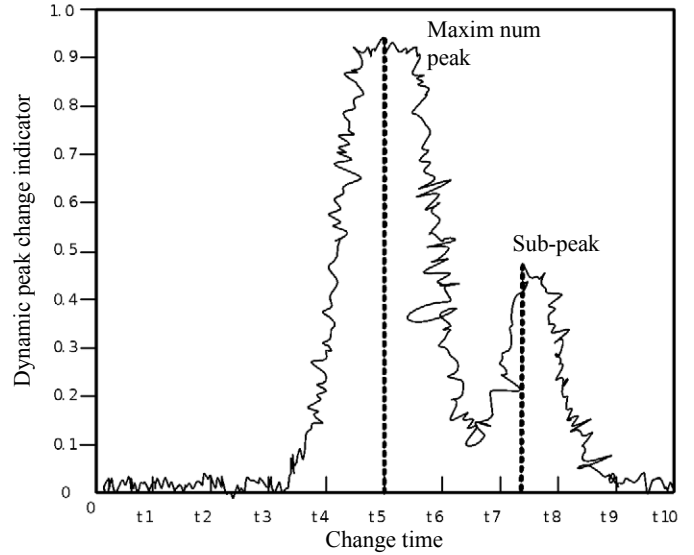

Figure 5. Fault peak curve

The selected fault samples need to meet the basic requirements of two peaks. The fault data of gears and bearings are "flat". Assuming that the abscissa of high peak value and sub peak value in "flat area" is x_1 and x_2, the center position c_0 and peak width L of the area are calculated. The calculation results are shown in the following formula:

$$\begin{cases} c_0 = \frac{|x_1 - x_2|}{sh} \\ L = \eta |x_1 - x_2| \end{cases} \tag{22}$$

In the formula, s is the number of peaks, and $s \ge 2$; h is the error correction coefficient; η is the width measurement parameter. According to the above calculation results, the distance between the fault node and the fault center position is determined. According to the real-time changing fault intensity indicator, combining Formulas 21 and 22, the random dynamic change parameter γ is calculated. The formula is:

$$\gamma = \frac{\varepsilon + d_0}{1 + \varepsilon} \times \frac{\alpha c_0}{L \cdot DFT} \tag{23}$$

In the above formula, ε is the adjustment control factor of defect peak; d_0 is the adjustment factor of dynamic parameter; α is the peak active direction of the fault with different intensity; DFT is the discrete transformation parameter. The linear regression model with activation function is as follows:

$$y(z) = \sum_{i=1}^{n} q_i(z)\omega_i + h(z) \qquad (24)$$

In the formula, n is the number of multi-peak defect nodes between gear and bearing; $y(z)$ is the expected output value; $q_i(z)$ is the calculation regression factor in the i-th fault section of gear or bearing; ω_i is the connection weight between fault nodes; $h(z)$ is the calculation residual. According to the model and the variation parameter γ, the defect center is obtained

$$c = \frac{\sum \gamma y(z)^2}{\sum y(z)^2} \qquad (25)$$

According to the obtained central coordinate position, the hardware fault edge is determined, and the specific range of fault position is obtained (Barrero et al., 2019). The boundary coordinates of the fault location are obtained by the least square method. According to the above calculation, the defect center c is obtained. Supposing there are n anchor nodes from the center. Within the determined fault target range, each coordinate can be represented by $a_1, a_2, ..., a_n$. Then, for each anchor node, there is $a_n = \{(x,y) \mid (x_1, y_1), (x_2, y_2), ..., (x_n, y_n)\}$, an unknown node is set as a_j, the node coordinate is (x_j, y_j), and the node is assumed to be the true coordinate of the fault. The relationship between the unknown node and the anchor node is:

$$\begin{cases} (x_j - x_1)^2 + (y_j - y_1)^2 = d_1^2 \\ (x_j - x_2)^2 + (y_j - y_2)^2 = d_2^2 \\ \vdots \\ (x_j - x_n)^2 + (y_j - y_n)^2 = d_n^2 \end{cases} \qquad (26)$$

$d_1, d_2, ..., d_n$ in the above formula represents the estimated distance between the unknown node and the anchor node. The coordinate boundary obtained by the formula is shown in Figure 6.
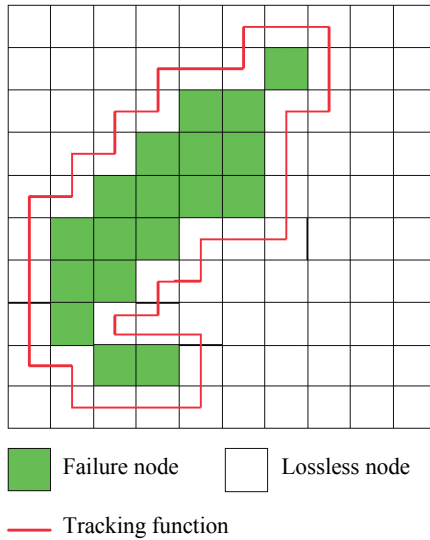

Figure 6. Obtained coordinates of fault boundary

It can be seen from the above figure that the gray area in the figure represents the true range of the fault, and the white area is the location of other nodes of the equipment affected by the fault. The boundary coordinates are obtained by the least square method. The formula (3-10) is rewritten into the

form of $Ax = b$, and the objective function $Min\|Ax = b\|^2$ is obtained by using the least square method

$$x = \begin{bmatrix} x_0 \\ y_0 \end{bmatrix} \qquad (27)$$

In the formula, x_0 and y_0 represent the abscissa and ordinate of the fault boundary respectively. Through the calculation process, the specific boundary coordinates of the fault in Figure 6 above are obtained, the influence scope of the fault in the mining equipment is determined, and the diagnosis mechanism of gear and bearing fault for mining equipment is studied under complex geological conditions (Vaziri et al., 2018).

Experimental study

In this paper, a comparative simulation experiment is proposed to simulate the complex geological environment in the process of coal mining (Yang et al., 2020). Opening the simulation test software, the bearing fault effect in the coal mining equipment is simulated. Table 2 below is the fault value to be simulated and the fault frequency parameters to be input (Wu et al., 2020).

Table 2. Simulated bearing failure frequencies

| Item Number	Fault frequency name	Failure frequency
A1	Rolling bearing outer ring failure frequency	162.178
A2	Rolling bearing inner ring failure frequency	227.822
A3	Rolling bearing rolling element failure frequency	86.593
A4	Failure frequency of cage touching inner ring	12.475
A5	Failure frequency of cage touching outer ring	17.525

Different bearing speeds are set. When the bearing speed is too high, the gear working frequency will be too high. At this time, the bearing signal indicators that cause bearing failure and gear failure are shown in Table 3 below.

Table 3. Indicator values of bearing vibration signals at different speeds

Different speeds and signals		Segment indicators				
Rotating speed	Signal	M1	M2	M3	M4	M5
800r/min	Normal 1	0.6055	0.4791	0.3451	0.2477	0.0342
	Normal 2	0.6012	0.4792	0.3487	0.2921	0.0371
	Internal loss 1	0.5805	0.4788	0.3561	0.2858	0.0475
	Internal loss 2	0.5865	0.4874	0.3563	0.2687	0.0411
	External loss 1	0.6345	0.4851	0.3522	0.2751	0.0480
	External loss 2	0.6327	0.4792	0.3566	0.2741	0.0382
1200r/min	Normal 1	0.6281	0.4853	0.3485	0.2736	0.0567
	Normal 2	0.6204	0.4722	0.3669	0.2819	0.0552
	Internal loss 1	0.5977	0.4621	0.3851	0.2654	0.0523
	Internal loss 2	0.5947	0.4673	0.3554	0.2647	0.0604
	External loss 1	0.6381	0.4615	0.3582	0.2708	0.0478
	External loss 2	0.6296	0.4628	0.3479	0.2432	0.0455

According to the data in the table above, the fault parameters of gears and bearings for coal mining equipment is simulated in a complex geological environment under high-intensity work. Two methods are used to analyze

the fault diagnosis mechanism. The proposed research method is used as the experimental group, and the traditional research method is used as the control group. The test results are shown in Figure 7 (Cheng et al., 2020).
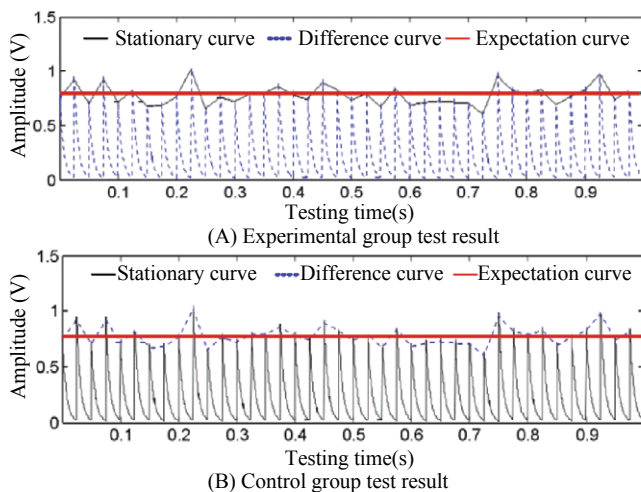
Figure 7. Experimental test comparison results

According to the curve trend in the figure above, it can be seen that the stability curve of the proposed research method is similar to the expected curve, while the stability curve of the traditional research method fluctuates violently, which is quite different from the expected curve. It can be seen that the stability difference value of the proposed research method is far lower than the stability difference value between the traditional research method and the expected curve (Gao et al., 2018).

Conclusions

In the complex geological environment, the proposed research method of fault diagnosis mechanism is more stable, which improves the reliability of diagnosis results and provides more perfect technical means for the development of national mining technology (Gao et al, 2019).

References

Ali, E. E., Teo, A. K. S., Goh, S. X. L., Chew, L., & Yap, K. Y. (2018). MedAd-AppQ: A quality assessment tool for medication adherence apps on iOS and android platforms. *Research in Social & Administrative Pharmacy*, 14(2018), 1125-1133.

Balestro, G., Festa, A., Borghi, A., Castelli, D., Gattiglio, M., & Tartarotti, P. (2018). Role of Late Jurassic intra-oceanic structural inheritance in the Alpine tectonic evolution of the Monviso meta-ophiolite Complex (Western Alps). *Geological Magazine*, 155(2), 233-249.

Barrero, L. H., Cifuentes, M., Rodríguez, A. C., Rey-Becerra, E., Johnson, P. W., Marin, L. S., Piedrahita, H., & Dennerlein, J. T. (2019). Whole-body vibration and back pain-related work absence among heavy equipment vehicle mining operators. *Occupational and Environmental Medicine*, 76(8), 554-559.

Cheng, H. Y., & Liu, Y. N. (2020). An improved RSU-based authentication scheme for VANET. *Journal of Internet Technology*, 21(4).

Ganson, T. (2018) Sensory malfunctions, limitations, and trade-offs. *Synthese*, 195(4), 1705-1713.

Gao, N. S., Cheng, B. Z., Hou, H., & Zhang, R. H. (2018). Mesophase pitch based carbon foams as sound absorbers. *Materials Letters*, 212, 243-246. DOI:10.1016/j.matlet.2017.10.074

Gao, N. S., Guo, X. Y., Cheng, B. Z., Zhang, Y. N., Wei, Z. Y., & Hou, H. (2019). Elastic Wave Modulation in Hollow Metamaterial Beam With Acoustic Black Hole. *IEEE Access*, 7, 124141-124146. DOI:10.1109/access.2019.2938250

Jeong, G. Y., Kong, J. H., Lee, S. J., & Pang, S. J. (2018). Comparisons of bearing properties for various oriented glulam using digital image correlation. *Journal of Wood Science*, 64(3), 1-9.

Heffner, J. L., Watson, N. L., McClure, J. B., Anthenelli, R. M., Hohl, S., & Bricker, J. B. (2018). "I Smoke Like This to Suppress These Issues That Are Flaws of My Character": Challenges and Facilitators of Cessation Among Smokers With Bipolar Disorder. *Journal of Dual Diagnosis*, 14(1), 32.

Liu, Y., Zhu, Z. Q. (2018). Influence of Gear Ratio on the Performance of Fractional Slot Concentrated Winding Permanent Magnet Machines. *IEEE Transactions on Industrial Electronics*, PP(99), 1-1.

Morris, Vachani, A., Pass, H. I., Rom, W. N., Ryden, K., Weiss, G. J., Hogarth, D. K., Runger, G., Richards, D., Shelton, T., & Mallery, D. W. (2018). Whole blood FPR1 mRNA expression predicts both non-small cell and small cell lung cancer. *International Journal of Cancer*, 142(2), S34-S34.

Sayers, E., Rich, J., Rahman, M., Kelly, B., & James, C. (2019). Does Help Seeking Behavior Change Over Time Following a Workplace Mental Health Intervention in the Coal Mining Industry? *Journal of Occupational and Environmental Medicine*, 61(6), 1.

Spartalis, M., Tzatzaki, E., & Spartalis, E. (2018). Letter by Spartalis et al Regarding Article, "Left Ventricular Assist Device Malfunctions: It Is More Than Just the Pump". *Circulation*, 137(21), 2298-2299.

Vaziri, V., Hamidi, J. K., Sayadi, A. R. (2018). An integrated GIS-based approach for geohazards risk assessment in coal mines. *Environmental Earth Sciences*, 77(1), 29.

Walker, T., Zahn, N., Bruckner, T., Streit, M. R., Mohr, G., Aldinger, P. R., Clarius, M., & Gotterbarm, T. (2018). Bruckner. Mid-term results of lateral unicondylar mobile bearing knee arthroplasty: A multicentre study of 363 cases. *Bone & Joint Journal*, 100-B(1), 42-49.

Wang, K. X., Huang, H., Liu X. D., & Pan, J. Y. (2018). Origin and influence of a Late Mesozoic multistage I- and A-type granitic complex in northern Fujian Province, South China. *Geological Journal*, 54(1), 39-61.

Wu, Z., Liu, Y. N., & Jia, X. X. (2020). A Novel Hierarchical Secret Image Sharing Scheme with Multi-Group Joint Management. *Mathematics*, 8(3), 12. DOI:10.3390/math8030448

Yang, F., Yang, F., Wang, G. Y., Kong, T., Wang, H., & Zhang, C. S. (2020). Effects of water temperature on tissue depletion of florfenicol and its metabolite florfenicol amine in crucian carp (Carassius auratus gibelio) following multiple oral doses. *Aquaculture*, 515, 9. DOI:10.1016/j.aquaculture.2019.734542